SUPPLEMENTARY MATERIALS

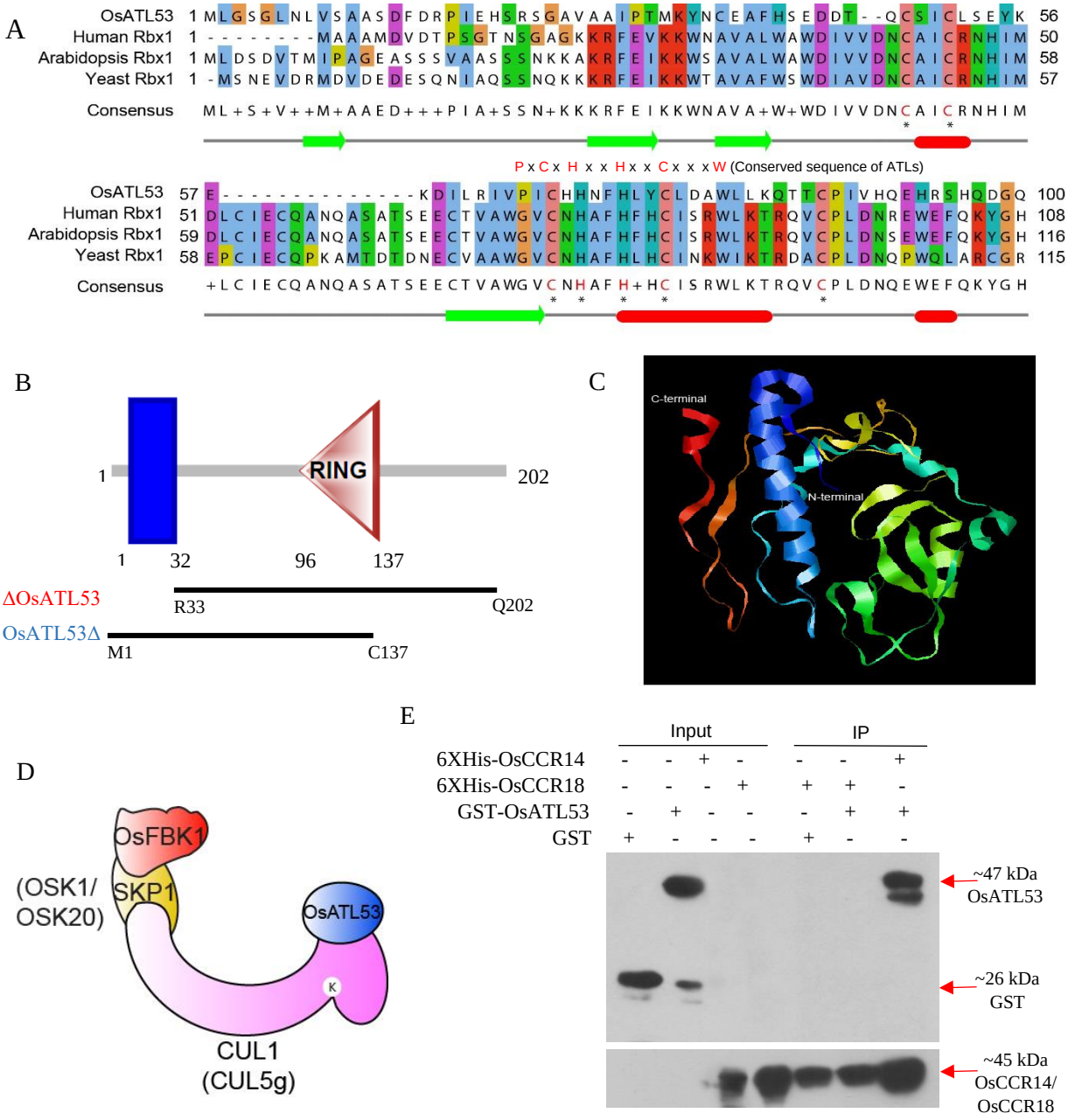

Fig. S1. Structural analyses of OsATL53. A: MAFFT alignment of the protein sequences of OsATL53, human, *Arabidopsis* and yeast RBX1. The consensus and canonical domain sequences of RBX1 have been highlighted in red with black asterisks. The red asterisks denote the hallmark residues of ATL RING-H2 proteins. Green arrows denote α-helices and red bars depict β-sheets. **B:** SMART prediction of the domains present in OsATL53. The N-terminal end contains a transmembrane domain from 10-32 aa position that is usually present in ATL RING-H2 proteins. The hallmark RING-H2 domain is present towards the C-terminal end (96 to 137 aa). The start and end amino acids of the OsATL53 deletion constructs are also shown. **C:** Ab initio modelled putative protein structure of OsATL53. **D.** Graphical representation of a putative SCF^{OsFBK1} complex complete with OsATL53. **E.** IP between OsCCR18-OsATL53. Positive control: OsCCR14-OsATL53 IP. Related to Fig. 1.

A

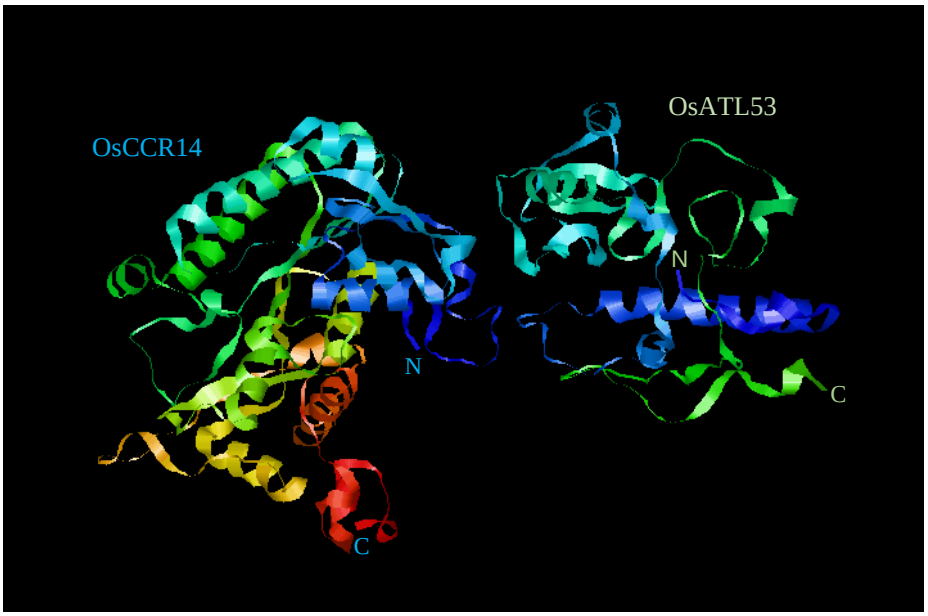

B

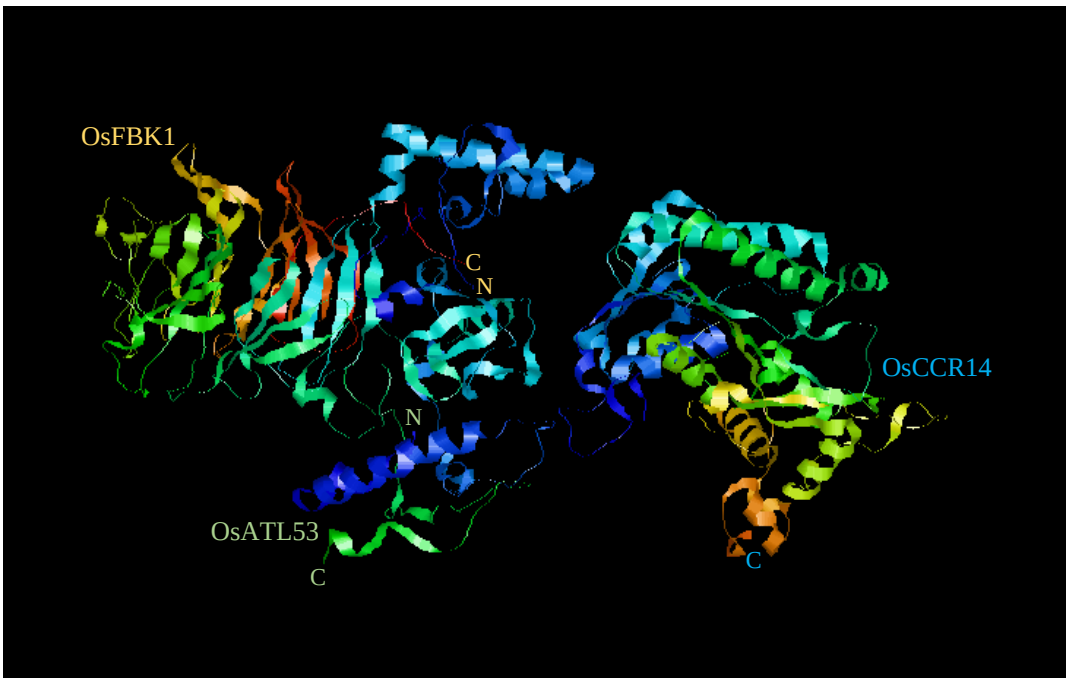

Fig. S2. Predicted putative protein complexes. A: OsCCR14 and OsATL53, and **B:** OsFBK1, OsATL53 and OsCCR14. N – N-terminal end, C - C-terminal end.

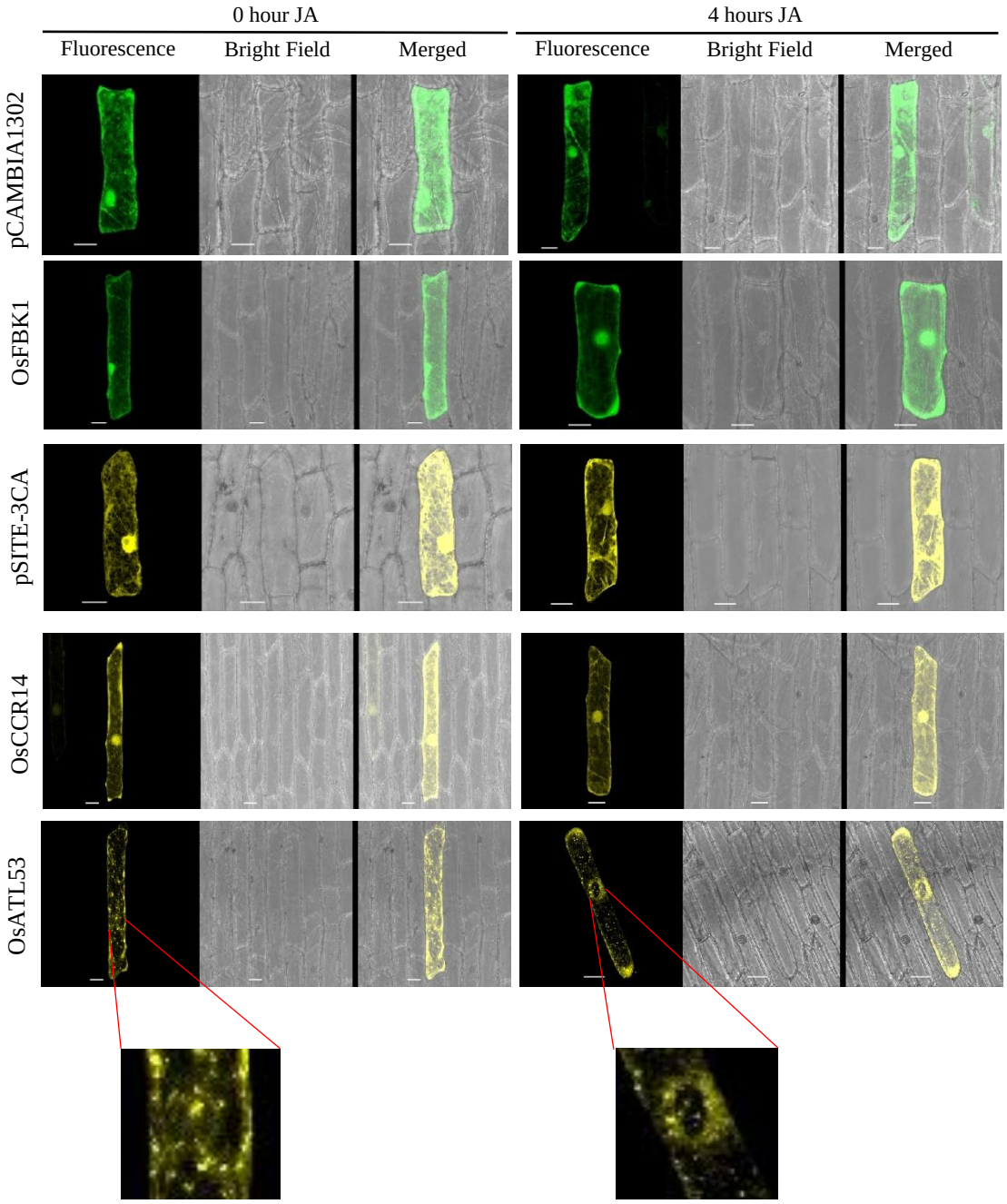

Fig. S3. Sub-cellular localization of proteins under control and JA treatments. The localization patterns of the vector controls, OsFBK1 and OsCCR14 are unaffected even after 4 h of JA treatment. However, OsATL53 shows a slight increase in accumulation around the nucleus after 4 h of JA treatment. The inset pictures show the nucleus and the fluorescence around it. Bar- 50 µm. Related to Fig. 3.

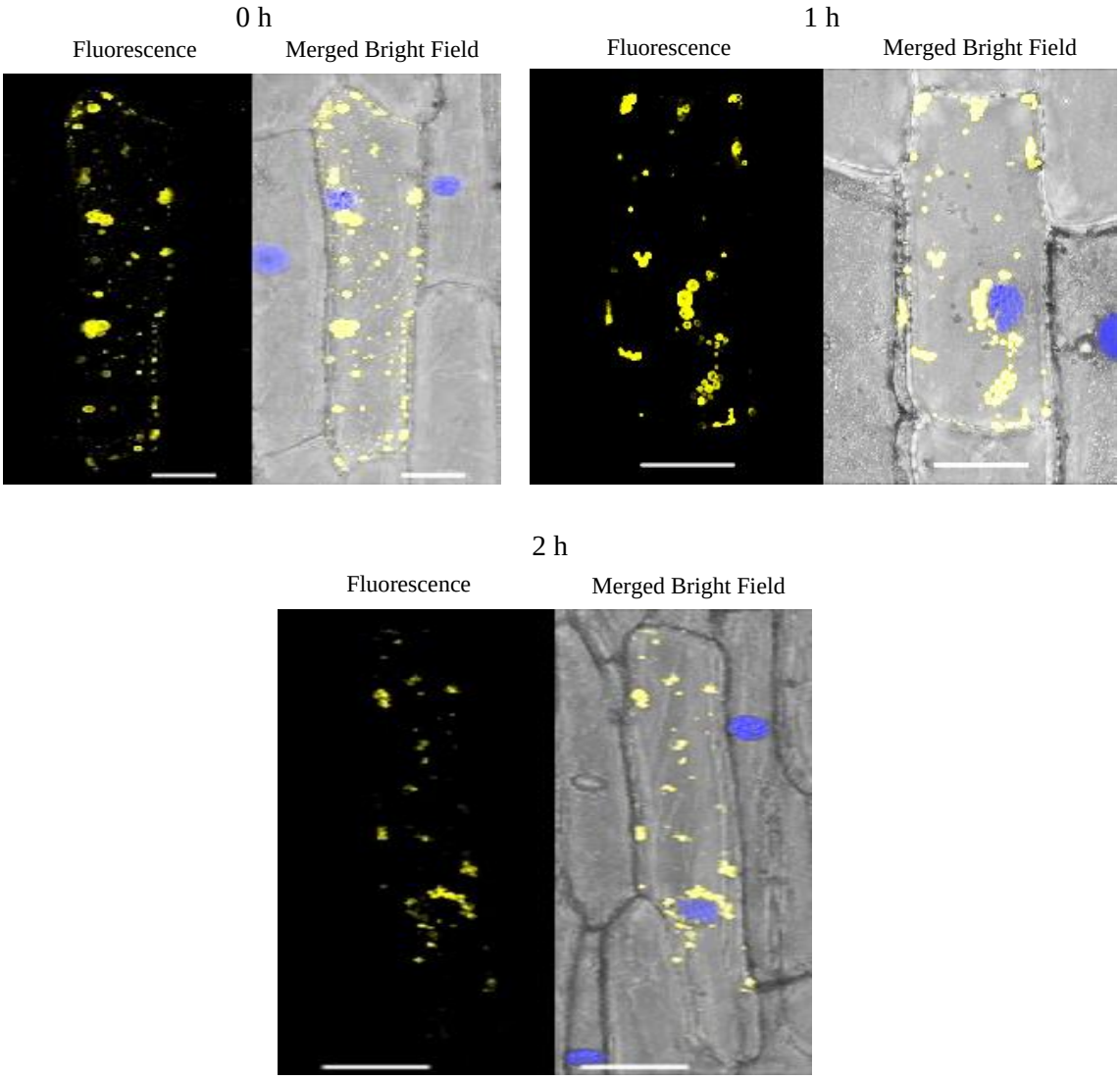

Fig. S4. Sub-cellular localization of OsCCR14+OsATL53 BiFC complexes under control and JA treatments with nuclear stained cells. DAPI stained nuclei are shown in the merged Bright field images. Bar- 50 µm. Related to Fig. 3.

A

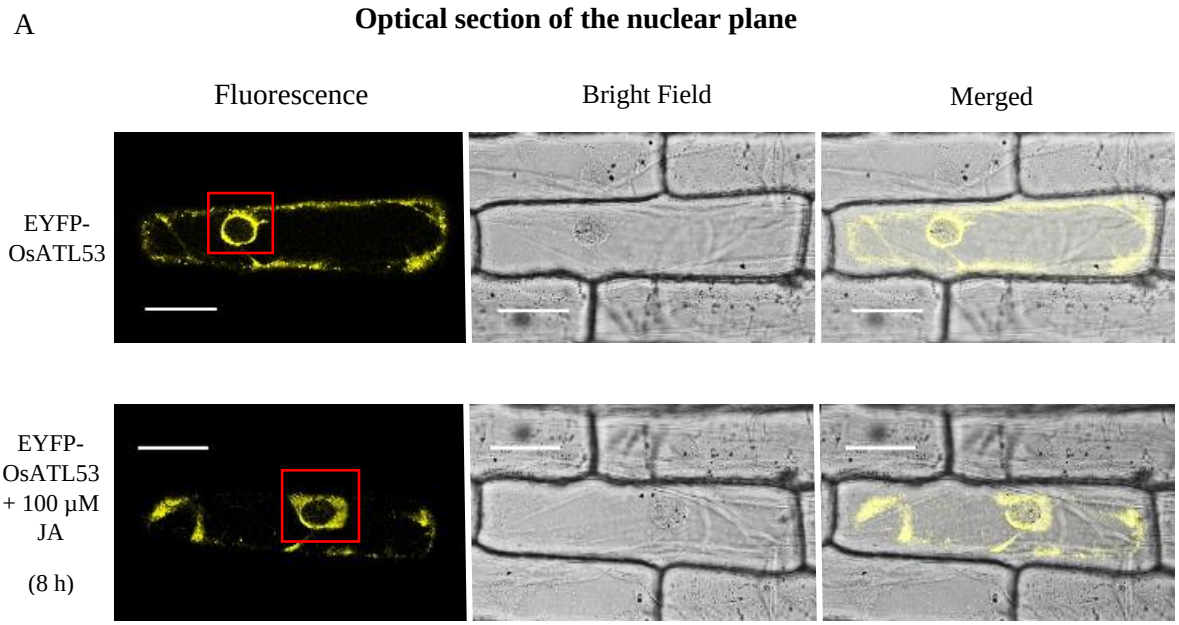

B

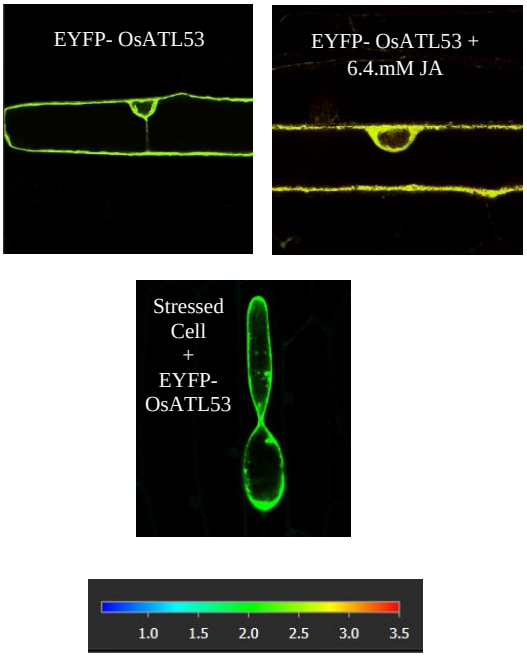

C

Donor Constructs	Avg. Lifetimes (ns)	Standard Deviation
EYFP-OsATL53	2.97885	0.040463
EYFP-OsALT53 + 6.4mM JA (4 h)	3.048	0.107731
Stressed cell + EYFP-OsATL53	2.593	0.0986

Fig. S5. Sub-cellular localization of OsATL53 under different JA concentrations. A: Initiation of accumulation of EYFP-OsATL53 around the nucleus of a representative target cell when exposed to 100 µM JA for 8 h. The accumulation is highlighted by the red boxes. **B:** Representative Fast-FLIM images of the nuclear plane of cells expressing EYFP-OsATL53 before and after exposure to 6.4 mM JA for 4 h respectively. No changes in lifetime of fluorophore observed. Plasmolysed cells display decrease in lifetime of EYFP-OsATL53 due to changes in cell integrity. **C:** Calculated average lifetimes (ns) of 5 observed cells before and after JA treatment. Bar – 50 µM. Related to Fig. 3.

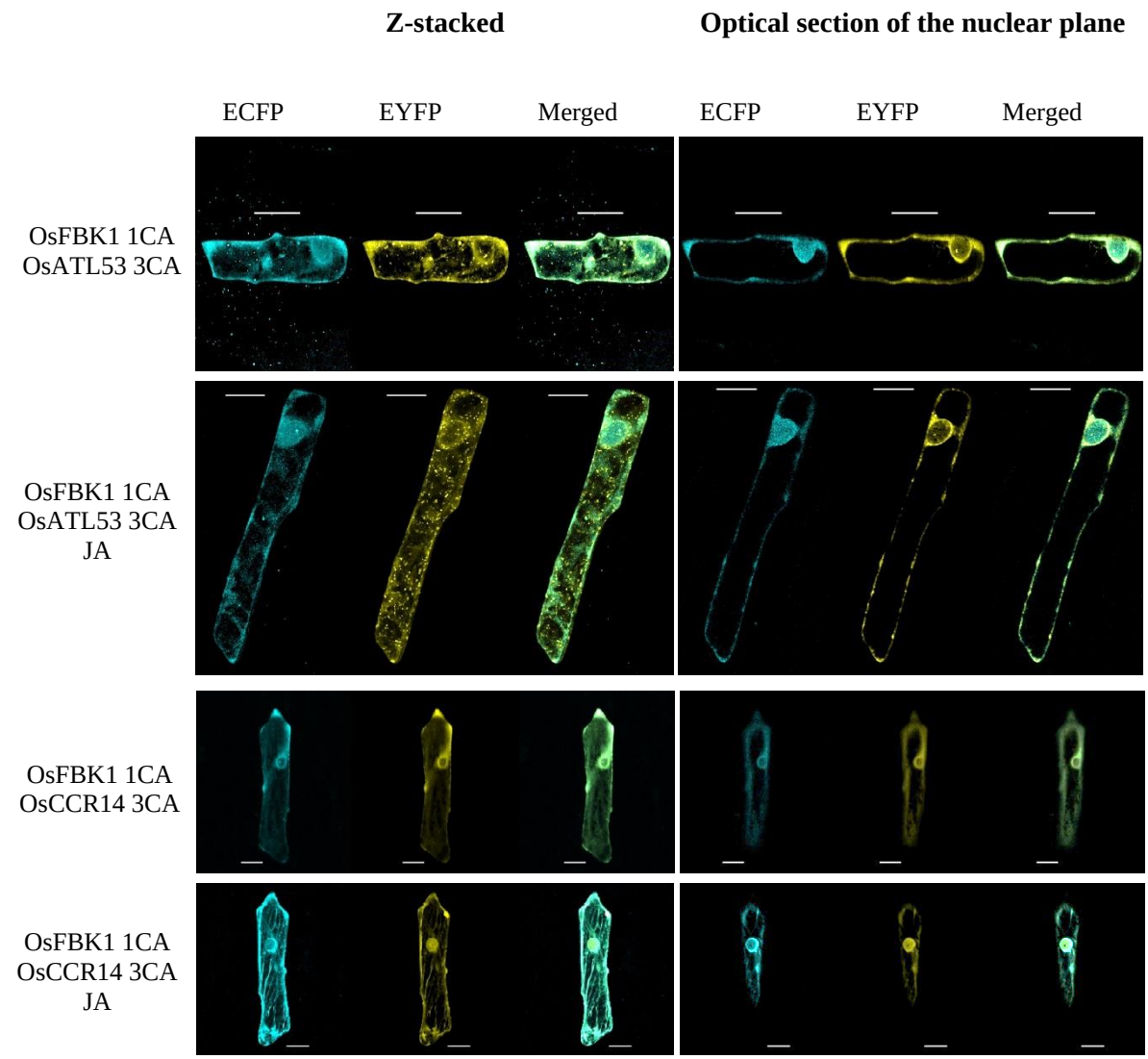

Fig. S6. Sub-cellular co-localization of OsFBK1-OsATL53 under control and JA treatments. The co-localization patterns of OsFBK1-ECFP and OsATL53-EYFP are unaffected even after 4 h of 6.4 mM JA treatment. The same is true for OsFBK1-ECFP and OsCCR14-EYFP (lower two panels). The panels on the right show the plane that is an optical section of the nucleus. Bar- 50 µm. Related to Fig. 3.

A

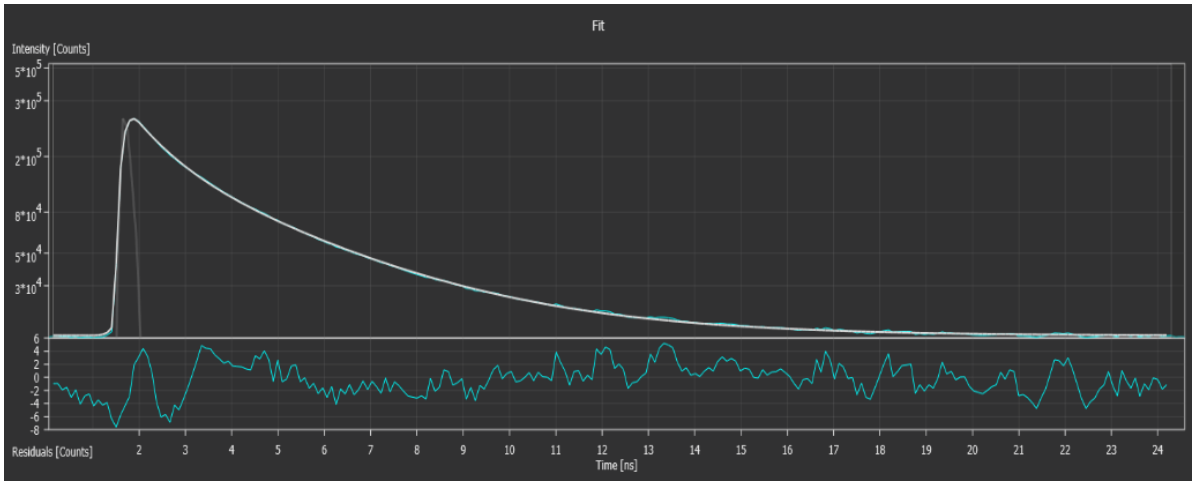

B

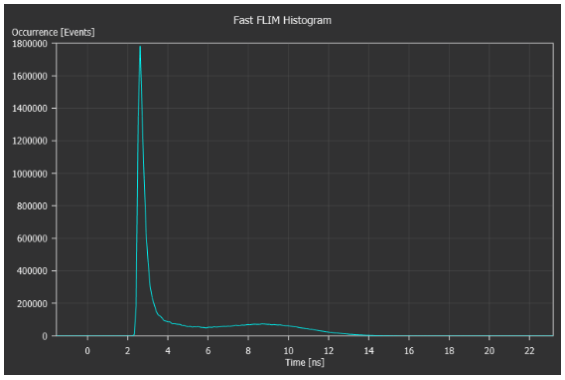

C

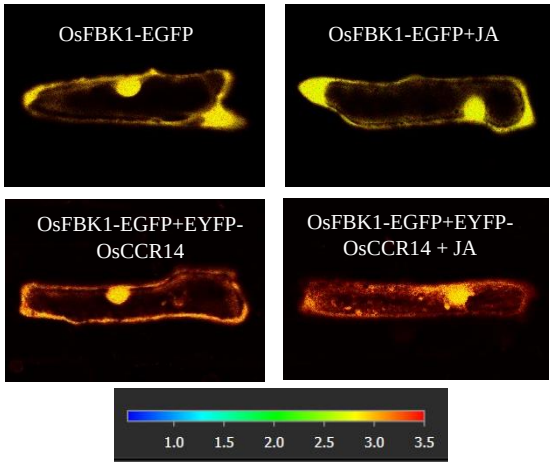

D

Donor Constructs	Avg. Lifetimes (ns)	Standard Deviation
OsFBK1-EGFP	2.873	0.08912
OsFBK1-EGFP+ JA	2.7528	0.0264
OsFBK1-EGFP (EYFP-OsCCR14)	2.6835	0.1083
OsFBK1-EGFP (EYFP-CCR14) +JA	2.7004	0.0648

E

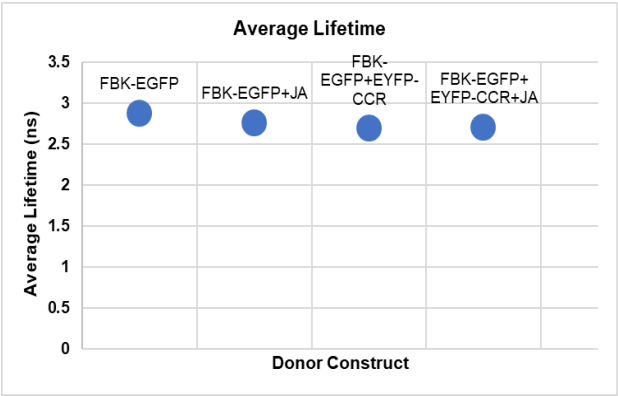

Fig. S7. Additional FLIM-FRET data. A: Representative image of curve fitting of FLIM data by n-Exponential Reconvolution fit model that shows statistical fitness of donor lifetime. **B:** Representative Fast-FLIM Histogram showing the number of counts of photons captured during FLIM. **C:** Representative Fast-FLIM images of target cells with control donor construct (OsFBK1-EGFP) in different conditions. Bar- range of lifetimes from 0.5-3.5 ns. **D:** Lifetime data of control construct. **E:** Graphical representation of lifetimes of a minimum of 5 cells with OsFBK1-EGFP donor construct (control) under different conditions. Reported lifetime of EGFP is 2.6 ns in solution. Related to Fig. 3.

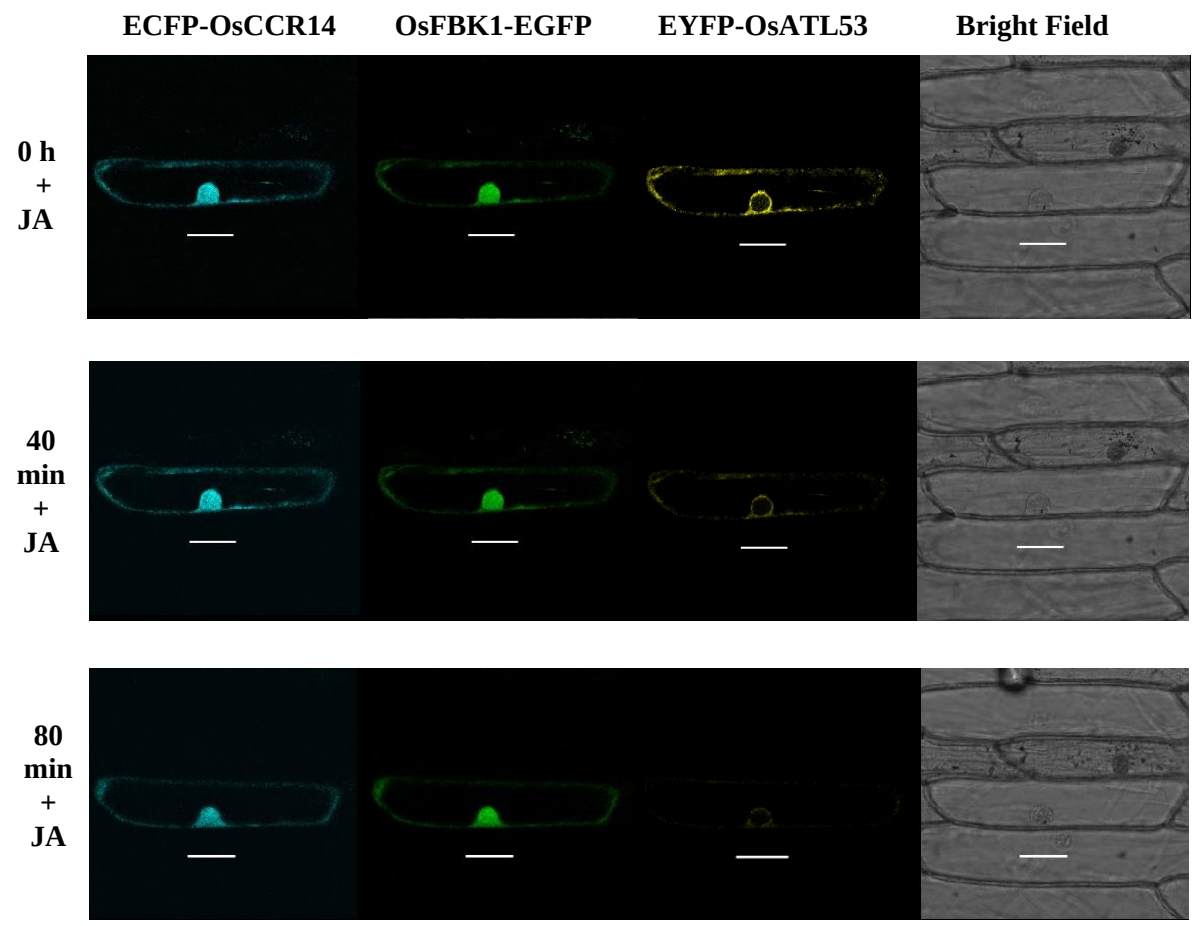

Fig. S8. Time-lapse confocal images depicting the targeted degradation of EYFP-OsATL53 in the presence of 6.4 mM JA. No apparent differences in signals were seen for ECFP-OsCCR14 and OsFBK1-EGFP. Bar – 50 µm. Related to Fig. 4.

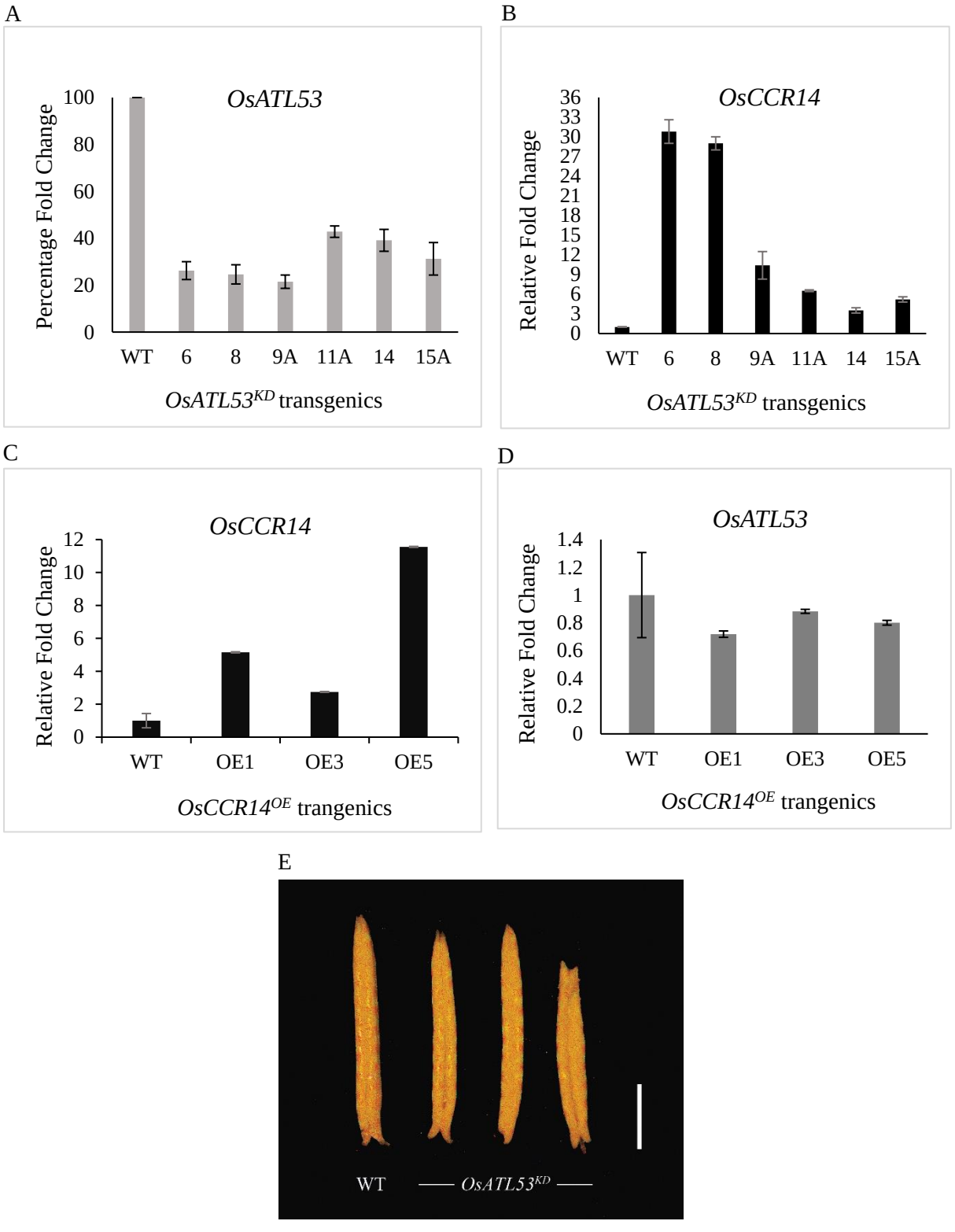

Fig. S9. Real-time expression analyses. **A.** Expression level of *OsATL53* in *OsATL53*^{KD} rice transgenics showing down-regulation. **B.** *OsCCR14* expression in *OsATL53*^{KD} displaying up-regulation. **C.** Expression of *OsCCR14* in *OsCCR14*^{OE} *transgenics*. **D.** *OsATL53* expression in *OsCCR14*^{OE} transgenics. **E.** Anther morphology of *OsATL53*^{KD} rice transgenics w.r.t. WT. Bar – 2 mm. Related to Fig. 6.

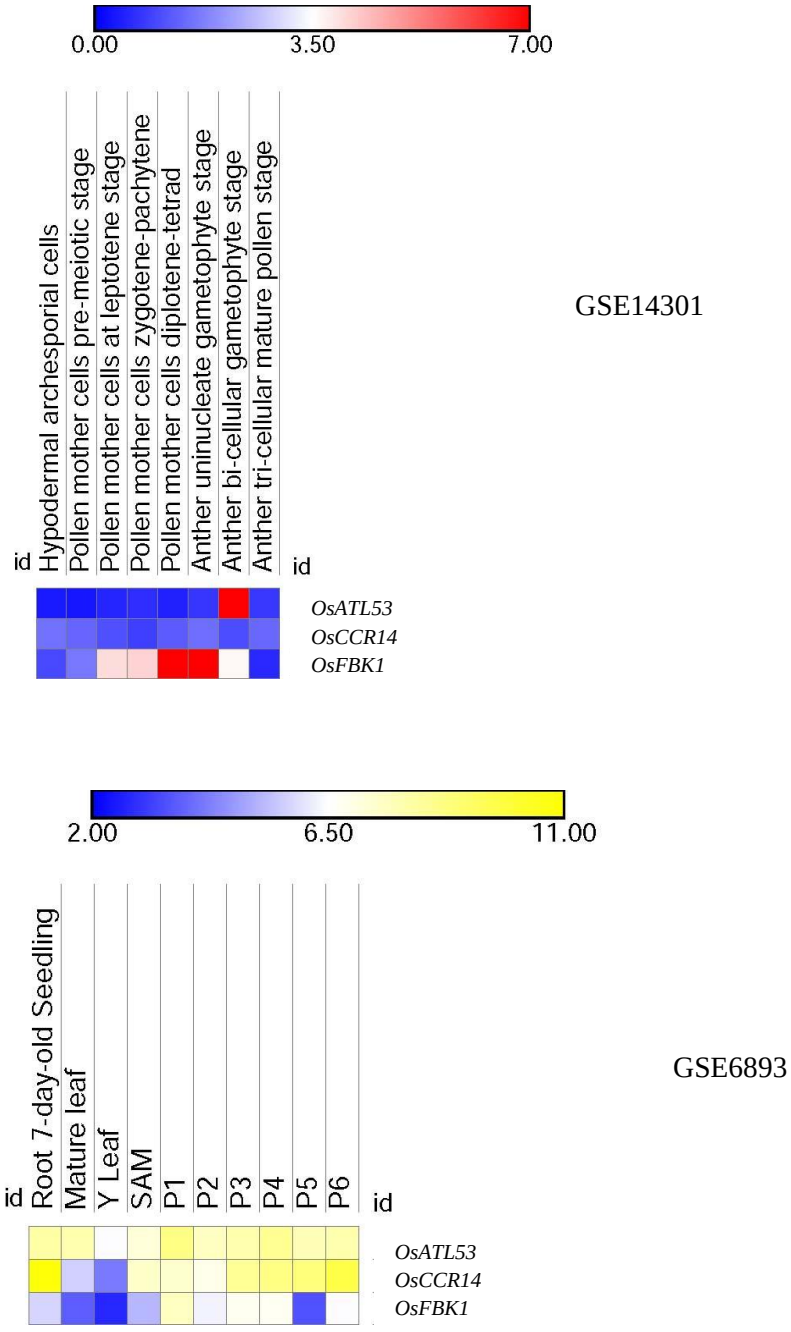

Fig. S10. Microarray expression data of *OsFBK1*, *OsCCR14* and *OsATL53* in different stages of rice development.

Table S1. Primers used in the study

Gene	Vector	Sequence
CUL5g	pGEX4T1	F: 5' ATAGGATCCATGGCGGGGCAGGAGCGG 3' R: 5' ATTGTCGACTCAAGCCAGGTATCTGTACACA 3'
OsATL53	pET28a	F: 5' ATAGAATTCATGCTGGGGTCGGGCCTGAA 3' R: 5' GCAGAGCTCTCACTGTCGGATTTCAATAACCAC 3'
	pENTR-D-TOPO	F: 5' CACCATGCTGGGGTCGGGCCTGAATCTCGT 3' R: 5' TCACTGTCGGATTTCAATAACCACCTCTA 3'
	pGEX4T1	Released from pET28a clone using *Eco*RI/*Sal*I
ΔOsATL53	pGEX4T1	F: 5' ATTGAATTCATGTTCGTCTGCTGCCGCGCC 3' R: 5' GGACTCGAGTCACTGTCGGATTTCAATAAC 3'
OsATL53Δ	pGEX4T1	F: 5' ATAGAATTCATGCTGGGGTCGGGCCTGAA 3' R: 5' ATACTCGAGTCAGCATATTGGGCAAGTAGTCTG 3'
OsCCR18	pET28a	F: 5' ATAGGATCCATGACCGTCGTCGTCGTTG 3' R: 5' AGGAAGCTTTCATGCTGGCACACCATTC 3'
At4CL1	pET28a	F: 5' ATAGGATCCATGGCGCCACAAGAACAAG 3' R: 5' GCTAAGCTTTCACAATCCATTTGCTAGTT 3'
OsATL53 real-time		F: 5' CCTCTGCTCCTACCATGTCTCA 3' R: 5' TGGTGGCTTCTGTGTTCTTGAT 3'
OsCCR14 real-time		F: 5' GCATCCTCGCCAAGCTCTT 3' R: 5' GGAGCTTCTGGTTCGACATCTT 3'
OsATL53 RNAi	pANDA	F: 5' CACCGAACACAGAAGCCACCAGGAT 3' R: 5' CTCTAGTCTACAACTTGCAAAGGGACC 3'
OsCCR14 ^{OE}	pMDC32	F: 5' CACCTCGTTCATCAAGATGACCGTGA 3' R: 5' TTGCTCTGCTGTTTTCCTCATGCTCGG 3'

MATERIALS AND METHODS

In silico analysis of OsATL53

The structure of OsATL53 (LOC_Os04g48310) was determined using the ROSETTA-based *ab initio* modelling server ROBETTA (http://robetta.bakerlab.org/). Ramachandran analysis of the obtained PDB was performed using the options available at the MOLProbity server (http://molprobity.biochem.duke.edu/). Visualization of the structure was carried out using the RasMol Molecular Graphics Visualisation Tool (http://rasmol.org/). To determine the RING-H2 domain region, the sequence of OsATL53 was analysed using SMART (Simple Modular Architecture Research Tool; http://smart.embl-heidelberg.de/), SWISS-MODEL Workspace (http://swissmodel.expasy.org/),

Phytozome v9.1 (http://www.phytozome.net/) and Pfam (http://pfam.sanger.ac.uk/). The consensus sequence of the RING-H2 domain was generated by aligning the protein sequence of OsATL53 with the sequences from Human (NP_055063), *Arabidopsis* (AT5G20570) and Yeast (NP_014508) using the MAFFT server (Multiple Alignment with Fast Fourier Transform; http://mafft.cbrc.jp/alignment/software/). The alignment was visualised in Jalview (http://www.jalview.org/) and curated to remove gaps and redundant sequences.

Prediction of putative protein complexes

Docking and prediction of putative protein complexes were carried out by using the freely available PRUNE and PROBE webserver (http://pallab.serc.iisc.ernet.in/prune/) (Mitra and Pal, 2011a, b). Ramachandran analyses of the obtained PDB files of the predicted complexes were performed using the options available at the MOLProbity server (http://molprobity.biochem.duke.edu/).

Cloning and induction of OsCCR18

OsCCR18 (LOC_Os09g25150, *OsCCR19* as per Kawasaki et al., 2006) was cloned in pET28a vector (*Bam*HI/*Hin*dIII) and mobilised into BL21-RIL competent bacterial cells for protein induction with 0.4 mM IPTG at 16^{o}C, 200 rpm, 16 h. The induced protein (~45 kDa) was found in the supernatant fraction and used for immunoprecipitation experiments as described earlier.

SUPPORTING REFERENCES

1. Mitra, P. & Pal, D. (2011a) Using correlated parameters for improved ranking of protein-protein docking decoys. J Comput Chem. 32(5):787-796.
2. Mitra, P. & Pal, D. (2011b) PRUNE and PROBE-two modular web services for protein-protein docking. Nucleic Acids Res. 39 (Web Server Issue): W229-34.